Toughening with Little Stiffness Loss: Polyamide Filled with ABC Triblock Copolymers

Laurent Corté,*,†,§ Valéry Rebizant,⊥,† Gilles Hochstetter,‡ François Tournilhac,† and Ludwik Leibler†

Matière Molle et Chimie, Ecole Supérieure de Physique Chimie Industrielles (UMR ESPCI-CNRS 7167), 10 rue Vauquelin 75231 Paris Cedex 05, France, and CERDATO, Arkema, 27470 Serquigny, France

Received May 15, 2006; Revised Manuscript Received September 28, 2006

ABSTRACT: In semicrystalline polymers, important toughening is obtained with dispersions of rubber particles. However, adding rubber most often induces a substantial loss in elastic modulus. In the present study, we investigate how to avoid such softening by using ABC triblock copolymers with low rubber content. A polyamide-12 matrix is toughened with polystyrene-*block*-polybutadiene-*block*-poly(methyl methacrylate) (SBM) triblock copolymers containing less than 40 wt % of rubber. We compare the mechanical properties of such systems to those of polyamide-12 toughened with pure reactive rubber. Impact properties are characterized by instrumented Charpy testing and post-mortem observations of crack surfaces. We report that dispersions of 10−20 wt % of SBM improve remarkably the impact strength, even at low temperature, without altering the elastic modulus of the polyamide matrix. Microscopic observations suggest that the large differences in impact strength between pure rubber and SBM-filled polyamide arise from differences in particle size and cavitation stress. Three-point bending measurements and dynamic mechanical analysis show that the high modulus of polyamide toughened with SBM is directly related to the low rubber content of the SBM copolymer and that softening also seems to be attenuated by the presence of hard glassy domains of S and M acting as stiffening agents.

Introduction

The impact performances of semicrystalline polymers including polyamides can be greatly enhanced by the incorporation of rubber fillers.[1−3] A strong toughening effect is achieved when the rubber phase forms a submicron-sized dispersion which is usually obtained thanks to reactive blending.[3,4] However, this toughening technique often requires a substantial concentration in filler of the order of 10−20 wt % which, in turn, implies a significant loss in elastic modulus. Using block copolymers instead of pure rubber is an interesting way to solve this issue.[5−9] The amount of rubber in the filler can be reduced by introducing glassy blocks while fine dispersions of block copolymers can still be achieved through reactive blending. For example, Oshinski et al. showed that dispersing 20% of maleated polystyrene-*block*-poly(ethylene−butene)-*block*-polystyrene triblock copolymers yields as much toughening as 20% of pure rubber. Hence, toughening can be obtained out of block copolymers dispersions. Still, most block copolymers used in previous works are rather soft with about 60−70 wt % of rubber. A question arises whether it is possible to achieve a substantial toughening with the help of block copolymers that contain only low fraction of rubber component. If such were the case, it should then be possible to achieve tough materials exhibiting high impact strength as well as high modulus. In the present study, we demonstrate the applicability of such a strategy to design tough and stiff polyamides by dispersing an ABC triblock copolymer containing less than 40 wt % of rubber.

Numerous studies have shown that the elastic modulus and impact strength of toughened systems can be tuned separately. On one hand, the overall elastic modulus of polymer blends is a function of the blend composition, morphology, and the elastic moduli of the components.[10−12] When particles are dispersed into a matrix as is the case here, the overall elastic modulus is mainly determined by the volume fractions and elastic moduli of both the matrix and the filler. The size of the dispersion does not have a significant effect.[13] On the other hand, experimental[13−21] and theoretical[22−26] studies show that the role of rubber in toughening of semicrystalline polymers is mostly related to the cavitation of the filler. The high dilative stresses produced in front of a growing crack induce the formation of voids in or around the rubber particles. As a result, hydrostatic pressure is relieved near the voids, and stress is redistributed in a cellular-like material. Cavitated particles act then as stress concentrators around which the matrix can deform plastically. Eventually, if the matrix is sufficiently confined between voided particles, plastic deformation extends in the whole material largely dissipating the impact energy. For given impact conditions, the minimum confinement that is required to induce ductile failure strongly depends on both the matrix nature[13,14,21] and the thermomechanical history.[27−29] Hence, as long as there is enough rubber to cavitate and promote toughening, it may not be necessary that the whole filler particle be of rubber.

Polystyrene-*block*-polybutadiene-*block*-poly(methyl methacrylate) (SBM) triblock copolymers are good candidates to fulfill the objectives of this study. Recently, Corté and Leibler reported that droplet coalescence is strongly inhibited when a SBM copolymer having a cocontinuous structure is dispersed into a polyamide matrix.[30] As a result, the formation of large droplets acting as critical defects is prevented, as opposed to usual immiscible blends. Moreover, if finer dispersions are required, acid groups can possibly be incorporated into the M block to form reactive polystyrene-*block*-polybutadiene-*block*-poly[(methyl methacrylate)-*stat*-(methacrylic acid)] (SB(MA)).[31,32] With such block copolymers, the rubber content is controlled by varying the size of the polybutadiene (B) middle block relative to that of the glassy polystyrene (S) and poly(methyl

* Corresponding author. E-mail: corte@nyu.edu
† UMR ESPCI-CNRS 7167.
‡ CERDATO.
§ New address: Center for Soft Matter Research, New York University, 4 Washington place, New York, NY 10003.
⊥ New address: DuPont de Nemours Luxembourg, Sàrl, L-2984 Luxembourg.

10.1021/ma061090g CCC: $33.50
Published on Web 12/05/2006

Table 1. Morphological and Mechanical Characteristics of the Blends Presented in This Study

		morphology		mechanical properties (20°C)			
reference	filler content	d_n[a] (μm)	L_n[a] (μm)	J[b] (kJ/m^2)	F_{max}[b] (N)	impact stiffness[b] (kN/m)	flexural modulus[c] (MPa)
neat PA12	0 wt %			16 ± 3	224 ± 14	68 ± 3	1283 ± 8
1	5 wt % EPRm	0.06 ± 0.05	0.35 ± 0.02	33 ± 8	256 ± 17	63 ± 1	na
2	10 wt % EPRm	0.09 ± 0.04	0.13 ± 0.02	49 ± 4	254 ± 4	57 ± 2	1083 ± 21
3	20 wt % EPRm	0.10 ± 0.04	0.11 ± 0.02	61 ± 6	207 ± 3	44 ± 1	896 ± 18
4	5 wt % SBM	0.29 ± 0.27	1.23 ± 0.2	19 ± 3	240 ± 15	71 ± 3	na
5	10 wt % SBM	0.31 ± 0.31	1.12 ± 0.2	74 ± 6	264 ± 7	70 ± 2	1237 ± 40
6	20 wt % SBM	0.35 ± 0.30	0.68 ± 0.2	113 ± 3	266 ± 3	65 ± 2	1173 ± 7

[a] Number-average diameter, d_n, and interparticle ligament thickness, L_n, are measured by image analysis of TEM micrographs.[33] Error ranges correspond to standard deviations. [b] Impact strength, J, maximum force at break, F_{max}, and impact stiffness are measured from instrumented notched Charpy impact testing. [c] Flexural modulus is obtained from three-point bending measurements.[31]

methacrylate) (M) end blocks. To reduce significantly the amount of rubber, we chose a symmetric composition where each component has the same molecular weight. Hence, dispersing 20 wt % of this SBM filler corresponds to an overall rubber content of only 7 wt %.

In the present paper, we investigate the mechanical properties of polyamide systems toughened with this SBM copolymer as compared to those of polyamide toughened with pure reactive rubber of maleated ethylene-*co*-propylene (EPRm). Unlike polyamide/EPRm or polyamide/SB(MA), polyamide/SBM is not a reactive blend, and the corresponding dispersions are rather coarse. Yet, impact testing and post-mortem observations of broken samples show that SBM dispersions remarkably improve the impact strength of polyamide including at low temperatures. The impact strength is even larger for SBM toughened systems than for state-of-art reactive rubber systems. More interestingly, these high impact performances are obtained with no or very little loss in elastic modulus as opposed to blends filled with pure reactive rubber, which are substantially softened. The nanostructure and composition of block copolymer particles govern both toughening efficiency and stiffness. In particular, dynamic mechanical analysis suggests that hard domains of glassy S and M blocks could act as stiffening agents which attenuate the softening due to the B rubber block.

Experimental Section

Materials. The semicrystalline polyamide-12 (PA) matrix with $M_n = 25$ kg/mol and $I_p = 2.3$ was provided by Arkema. Two impact modifiers were studied at various concentrations ranging from 5 to 20 wt %. The pure rubber filler consists of a reactive poly(ethylene-*stat*-propylene) copolymer (EPRm) (Exxellor VA1801, Exxon) with an ethylene/propylene ratio of 70/30 and 0.7 wt % of maleic anhydride. The block copolymer filler is a symmetric polystyrene-*block*-polybutadiene-*block*-poly(methyl methacrylate) triblock copolymer (SBM) (Arkema) containing about 30 wt % of residual SB diblock coming from the synthesis. The overall composition of the block copolymer mixture is 32 wt % polystyrene (S), 36 wt % polybutadiene (B), and 32 wt % poly(methyl methacrylate) (M) with an effective number-average molecular weight of 94 kg/mol. The morphology development of PA/SBM blends is commented in more details elsewhere.[30] The morphological and mechanical characteristics of these systems are reported in Table 1. For each system, blending was achieved by extruding together the modifier and polyamide pellets in a corotating twin-screw extruder ZSK 30/41D (Werner & Pfleiderer) at a rotation speed of 300 rpm and a temperature of 250 °C.

Specimen Preparation. Standard test bars were injected according to ASTM/ISO requirements with dimensions of 80 × 10 × 4 mm^3. All injections were achieved on a Battenfeld 800DC injector in the same conditions of temperature, pressure, and speed. For Charpy impact testing, notches were cut with a CEAST Notchvis device according to the specifications of ISO179 given in Figure 1a.

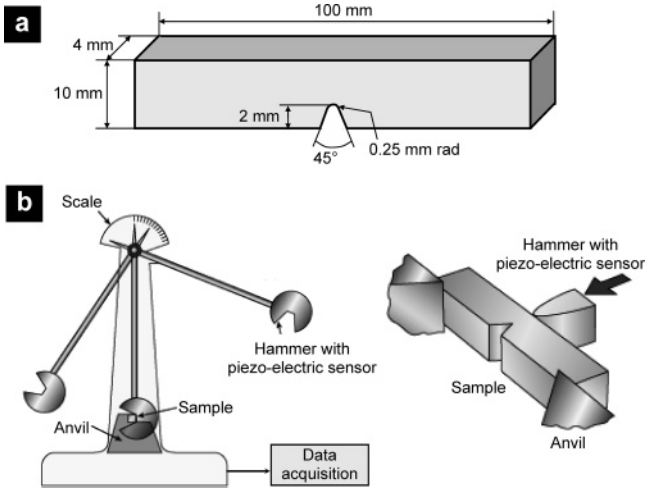

Figure 1. Standard Charpy impact testing. (a) Dimensions of notched test bars. (b) Schemes illustrating the instrumented device.

Morphological Characterization. Filler dispersions and nanostructures were characterized by transmission electron microscopy (TEM) using stained ultrathin sections. Ultrathin sections were cut with a Leica Ultracut UCT apparatus at −100 °C with a diamond knife. Osmium tetroxide (OsO_4) vapor was used to selectively stain butadiene in systems toughened with SBM. In the case of EPRm, the polyamide matrix was stained instead of the filler with a 4% aqueous solution of phosphotungstic acid (H_3PO_4, $12WO_3$). Experiments were carried out with a JEOL 100CX electron microscope at an acceleration voltage of 80 kV.

Impact Testing. Notched test bars were dried in a vacuum oven at 50 °C for 24 h and kept in a desiccator prior to impact testing. Impact response was studied by notched Charpy impact tests using an instrumented CEAST Resil Impactor apparatus. During the impact, this system measures both the time and the force applied by the test bar to the hammer, as illustrated in Figure 1b. Knowing the force $F(\tau)$ at any time τ, energy conservation gives the speed $v(t)$ and displacement $l(t)$ of the hammer at time t from the beginning of the impact as follows:

$$v(t) = v_0 - \frac{1}{m}\int_0^t F(\tau)\,d\tau \quad (1)$$

$$l(t) = \int_0^t v(\tau)\,d\tau \quad (2)$$

in which the time scale origin ($t = 0$) corresponds to the beginning of the impact, v_0 is the hammer speed at $t = 0$, and m is the hammer mass (1.2 kg). All tests were run at room temperature with a 5 J pendulum and an impact speed of $v_0 = 2.9$ m/s. Each measurement was repeated with at least four to five specimens in order to check the reproducibility of the test. For sake of clarity, we only show here one curve for each system.

Low-temperature measurements were carried out using a non-instrumented Charpy testing device which only measures the energy

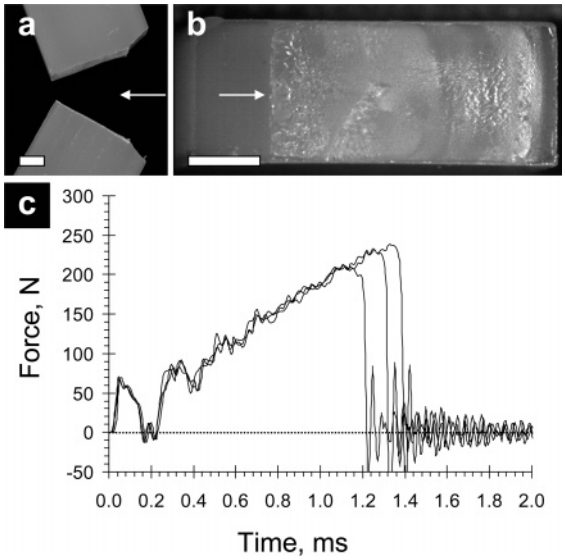

Figure 2. Impact behavior of pure polyamide-12. (a, b) Pictures of post-mortem samples show a side view (a) and a top view (b) of the crack surface. Arrows indicate the direction of the crack propagation. (scale bar = 2 mm). (c) Instrumented impact measurements showing the force as a function of time for three different samples.

dissipation. Before each measurement, the samples were stored in a temperature-controlled chamber for 30 min for thermal equilibration. Then, test bars were quickly removed one by one and installed on the testing apparatus. The testing protocol was defined to ensure that the testing temperature is well-controlled: the temperature of the chamber is set about 1 °C below the measurement temperature, and testing is done within a few seconds after the sample is taken out from the chamber.

Post-Mortem Observations. After impact testing, broken samples were characterized by optical and scanning electron microscopy (SEM). Pictures were taken with a digital camera installed on a Leica Wild MZ8 binocular. SEM experiments were realized at an acceleration voltage of 10 kV. Prior to these observations, samples were coated with a 2 nm thick gold−palladium layer.

Modulus Measurements. Three-point bending tests were realized on unnotched impact test bars according to the specifications of ISO 178:93 with a robotized Zwick 1465 dynamometer. Flexural modulus was measured at a temperature of 23 °C and a speed of 2 mm/min.

Dynamic mechanical analysis (DMA) was performed on a DMA 2980 apparatus. Measurements were done in the single cantilever geometry and under a deformation of 50 μm. Samples were cut out from Charpy test bars with dimensions of about $4 \times 10 \times 30$ mm^3. Elastic moduli at 1 Hz frequency were measured as a function of temperature from −140 to 190 °C at a heating rate of 2 °C/min. For each system, measurements were done twice to check the reproducibility.

Results

This section is organized as follows. First, we present the impact performances of polyamide-12 in its unmodified state (pure polyamide-12) and toughened with pure reactive rubber fillers (EPRm). These results are described in detail for completeness and to better emphasize the difference with block copolymer fillers which are presented afterward. In a last part, we compare the temperature dependence of the impact strength of all three systems.

Pure Polyamide-12. At room temperature and under standard notched Charpy conditions, failure of pure polyamide-12 is brittle as shown in Figure 2. Pictures a and b of post-mortem samples show the typical fracture surface obtained after this brittle failure. There is no macroscopic trace of plastic deformation near the crack flanks. Crack direction is rather straight with a rough surface. The evolution of the impact force as a function of time is given in Figure 2c. Three measurements illustrate the good reproducibility of the experiment. Several characteristic features of instrumented impact testing appear on these curves.[34,35]

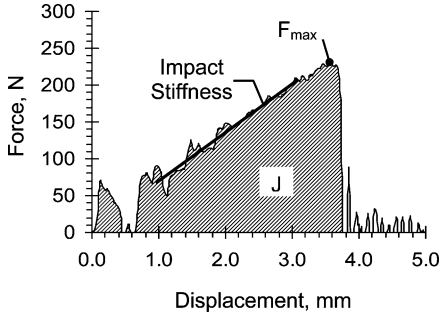

Figure 3. Force as a function of displacement for pure polyamide-12. The maximum force at break, F_{max}, the impact strength, J, and the impact stiffness are used to characterize the impact performance.

At the very beginning of loading, impact produces a sharp force spike. It corresponds to an inertial load which is required to accelerate the stationary sample to the speed of the hammer.[36]

As the hammer keeps on advancing, the test bar bends. The force increases rather linearly with many perturbations and oscillations. First, the specimen and hammer lose contact momentarily after the sharp inertial load. During this short period, both specimen and hammer oscillate at their natural frequencies. These oscillations persist in a forced vibration regime as the specimen and hammer get back in contact. These vibrations make the quantitative curve analysis delicate.[37] Here, their magnitudes have been reduced by applying a 0.3 mm thick film of soft plasticine on the tip of the hammer. Control tests showed that this procedure does not significantly alter the shape of the force curve in any other way than reducing the vibrations. Meanwhile and after the damping of oscillations, the force linearly increases with deformation, reflecting an elastic regime that corresponds to the bending of the test bar being pushed by the pendulum.

At about 1.2 ms, the load reaches a maximum, which may correspond to the initiation of the crack at the notch tip. At that point, the force suddenly drops to zero as a brittle crack propagates. It takes less than 0.1 ms for the crack to travel throughout the 8 mm thick sample. Thus, the crack speed is higher than 80 m s^{-1} and much greater than the hammer speed ($\sim$3 m s^{-1}). Such unstable crack propagation is most often characteristic of brittle failure while in the case of ductile failure, crack propagation is usually stabilized by plastic deformation and the crack advances as the hammer pushes the test bar. Last, after sample failure, harmonic oscillations of the load are still recorded owing to the hammer "ringing" at its own natural frequency.

Extensive studies have focused on the analysis and interpretation of instrumented impact tests in polymer materials.[37−40] Besides observations of crack surfaces, several quantities can be extracted from these measurements to characterize the impact behavior. However, they only reflect a global response of the sample and not the local phenomena occurring near the crack tip. In the following, we consider the maximum force at break, the impact strength and impact stiffness. They are illustrated in the case of polyamide-12 on the force−displacement graph given in Figure 3. The maximum force at break, F_{max}, is simply the maximum load attained before crack propagation. The impact strength, J, commonly designates the energy lost by the

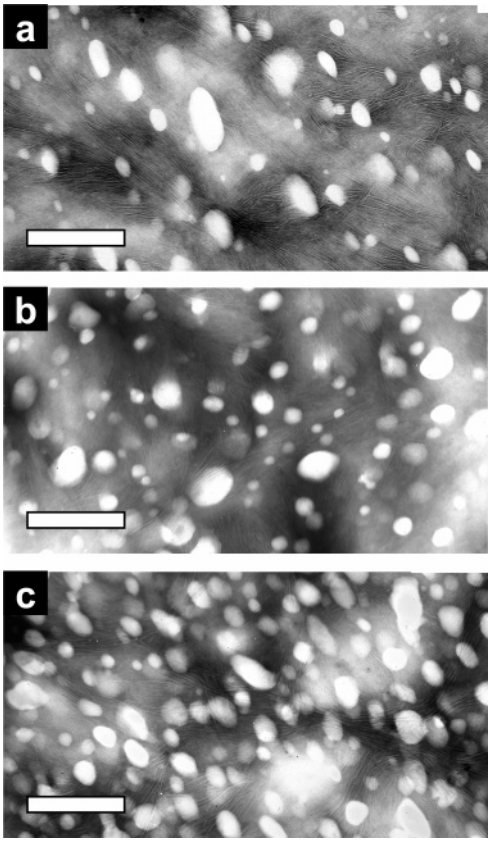

Figure 4. (a−c) TEM micrographs of polyamide-12 toughened with 5, 10, and 20 wt % EPRm, respectively (scale bar = 500 nm).

hammer during impact (area of the load−displacement curve) normalized by the area of the section behind the notch (∼32 mm^2). The impact stiffness is defined as the slope of the load−displacement curve measured between 0.3 and 1 ms, i.e., in the linear regime before crack propagation. It roughly characterizes the elastic modulus in the impact conditions. All these data are reported in Table 1 for the different toughened systems of this study. One must notice that they correspond to these particular impact conditions (temperature, hammer speed, sample geometry) and strongly depend on the thermomechanical and processing history of the samples.[27−29]

Polyamide Toughened with Pure Rubber (EPRm). TEM micrographs of EPRm dispersions are given in parts a, b, and c of Figure 4 for filler concentrations of 5, 10, and 20 wt %, respectively. Evidently, the number of particles increases while their size remains rather constant (∼100 nm). As particles keep evenly distributed even at high concentrations, the interparticle ligament thickness decreases from 350 nm at 5 wt % to 110 nm at 20 wt % (see Table 1). Pictures of post-mortem samples in Figure 5 illustrate the impact behavior of these systems. Fracture surfaces show that the failure mode progressively changes from semiductile to fully ductile. In all cases, the test bars do not break completely but undergo a hinge folding deformation and eventually slip through the anvil. Both halves of the broken test bars remain attached by a thin ligament. Whitened zones are visible on each side of the crack as the combined result of particle cavitation and extensive shear yielding of the matrix. We use this visual observation to distinguish ductile and brittle propagations. For the sample with 5 wt % EPRm shown in Figure 5a, a white region near the notch tip indicates that crack initiation and early propagation are ductile. However, crack propagation quickly becomes brittle as the white region ends after about 1 mm. After 2−3 mm of brittle crack propagation, another white region shows that failure is ductile again. This latter brittle-to-ductile transition is specific to bending tests like Charpy and Izod impact testing where loading conditions change as the crack propagates.[37] In particular, one-half of the test bar opposite to the impact point is under traction while the other half is under compression. The failure mode probably changed from brittle to ductile when the crack entered a region that had already been deformed plastically under compression. As the EPRm concentration is increased (Figure 5b,c), the white region near the notch tip becomes larger. Finally, crack propagation is fully ductile with 20 wt % EPRm.

Force measurements are given in Figure 6a−c. They correlate well with the surface observations of Figure 5. With 5 wt % EPRm, crack propagation is unstable like with pure polyamide-12. However, the maximum force at break is slightly increased from 230 to 260 N. Cavitation followed by plastic deformation at the notch tip probably delayed crack initiation. With 10 wt % EPRm, crack propagation is also unstable. After a sudden drop of the load, the hammer enters in its proper oscillatory regime, meaning that its tip is no longer in contact with the sample. Eventually, a small and broad signal appears, which corresponds to the hinge folding deformation around the unbroken ligament as the test bars slips through the anvil. Last, crack propagation is stable with 20 wt % EPRm as expected for a ductile behavior. Thus, crack propagation clearly becomes stable as the concentration in EPRm increases. These force measurements also show that toughening with EPRm is followed by an important softening. It is particularly clear in the insets of Figure 6. When EPRm content reaches 20 wt %, the impact stiffness characterized by the slope of the curve before crack propagation is significantly reduced (by a 0.7-fold factor) as compared to pure polyamide-12.

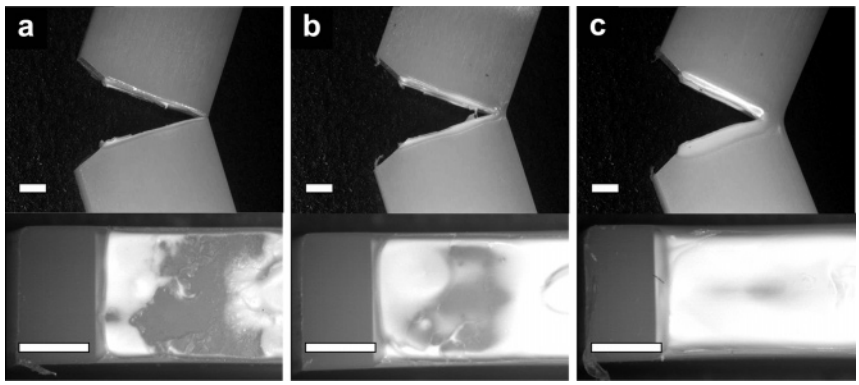

Figure 5. (a−c) Pictures of post-mortem samples polyamide-12 toughened with 5, 10, and 20 wt % of EPRm, respectively: side views (top row) and top views (bottom row) of crack surfaces (scale bar = 2 mm).

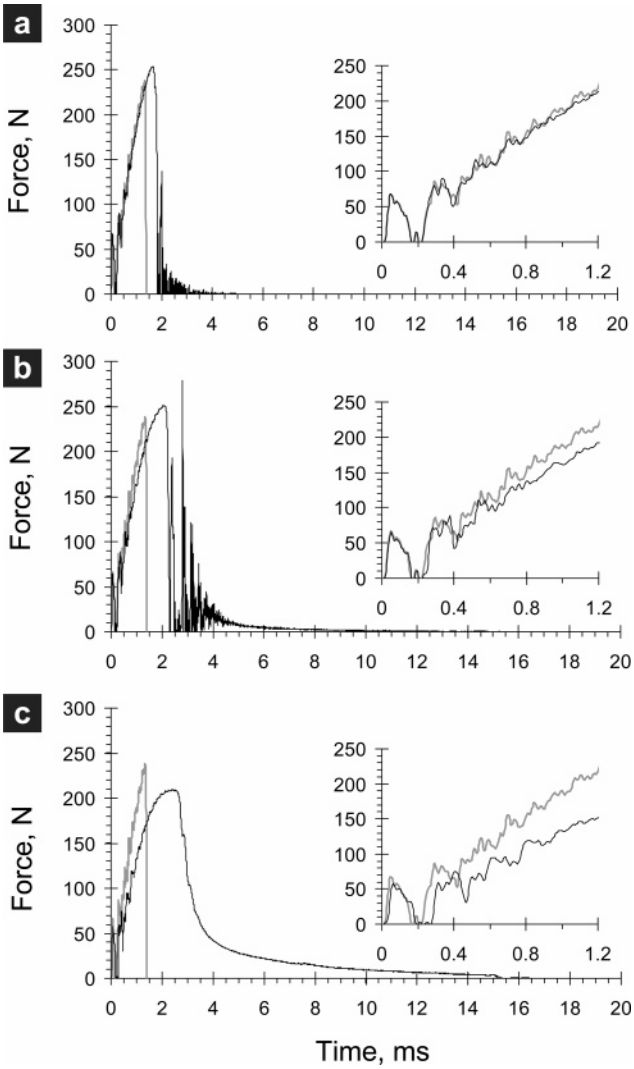

Figure 6. (a−c) Force vs time curves during impact testing for polyamide-12 toughened with 5, 10, and 20 wt % of EPRm, respectively. Gray curves on each graph show the reference behavior of pure polyamide-12. Close-ups of the linear loading regime before crack initiation are given in the insets.

Polyamide Toughened with SBM Triblock Copolymers. The situation is different in systems toughened with 5, 10, and 20 wt % SBM triblock copolymers. TEM micrographs of SBM dispersions are given in Figure 7a−c. Particle diameters and ligament thicknesses are much larger than in the case of EPRm modifiers. Unlike in Figure 4, the polyamide matrix is unstained here. Gray and bright shades reveal the crystalline texture of the matrix and correspond to regions where crystalline lamellae and amorphous layers have various orientations with respect to the thin film. As opposed to the EPRm filler that forms homogeneous rubber particles, the SBM particles exhibit an inner nanostructure due to the self-assembling of the SBM block copolymer chains. A high-magnification TEM micrograph given in Figure 8 shows the cocontinuous and irregular structure of one SBM particle embedded into the PA12 matrix. Staining with OsO_4 vapor reveals that dark stained B and gray S domains form cocontinuous domains that wrap bright M domains. The dispersion and morphology of these SBM block copolymers are described more precisely elsewhere.[30]

Pictures of post-mortem samples and fracture surfaces are given in Figure 9. Like in EPRm toughened samples, the failure mode progressively changes from semiductile to ductile as the SBM content increases. With 5 wt % SBM, cavitation and

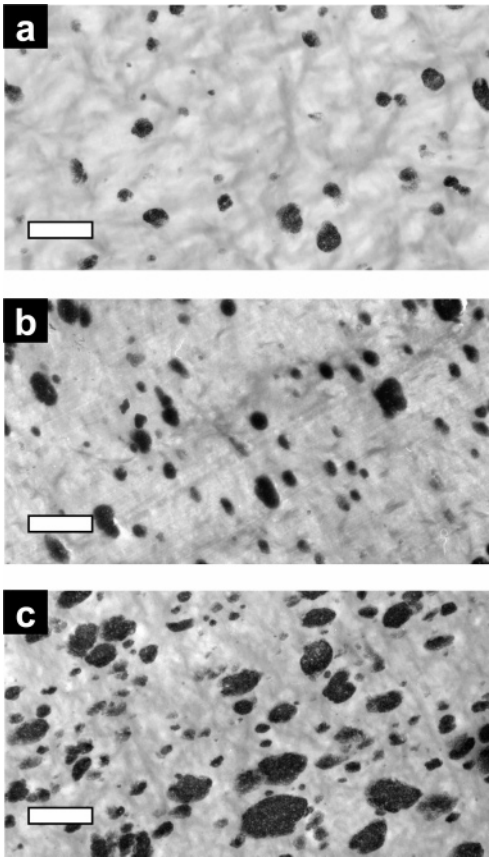

Figure 7. (a−c) TEM micrographs of polyamide-12 toughened with 5, 10, and 20 wt % SBM, respectively (scale bar = 2 μm).

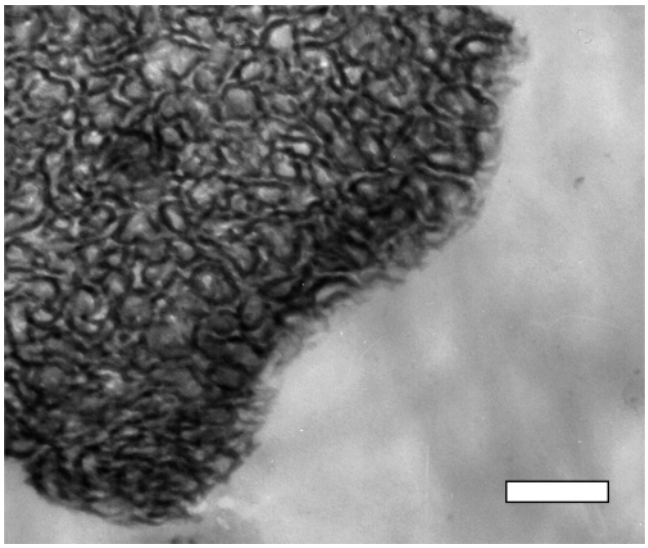

Figure 8. TEM micrograph showing the cocontinuous nanostructure of an SBM particle embedded into the PA12 matrix (scale bar = 250 nm).

plastic deformation are visible in front of the notch, as shown in Figure 9a. It is more developed near the sides of the test bars where plane stress conditions are dominant. However, crack propagation quickly becomes brittle. After a few millimeters, crack branching often occurs as indicated by arrows in Figure 9a. This phenomenon is known to appear at high crack speeds, which is consistent with unstable crack propagation.[41] For 10 and 20 wt % SBM, failure is fully ductile. Samples do not break completely. Extensive cavitation and plastic deformation take place in a large whitened volume on both sides of the crack.

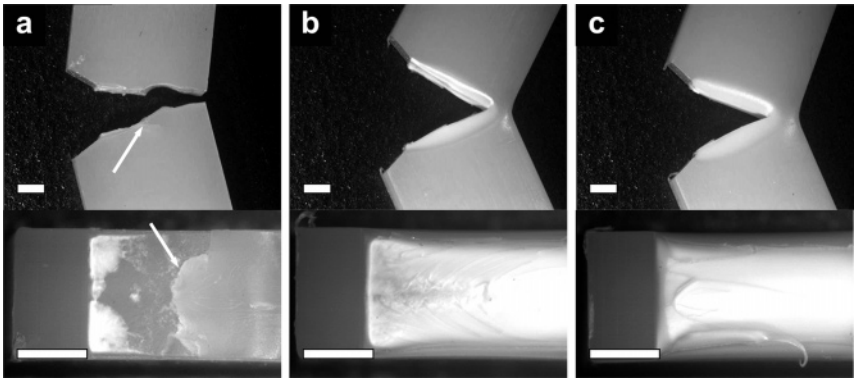

Figure 9. (a−c) Pictures of post-mortem samples polyamide-12 toughened with 5, 10, and 20 wt % of SBM, respectively: side views (top row) and top views (bottom row) of crack surfaces. Arrows in (a) indicate the onset of crack branching (scale bar = 2 mm).

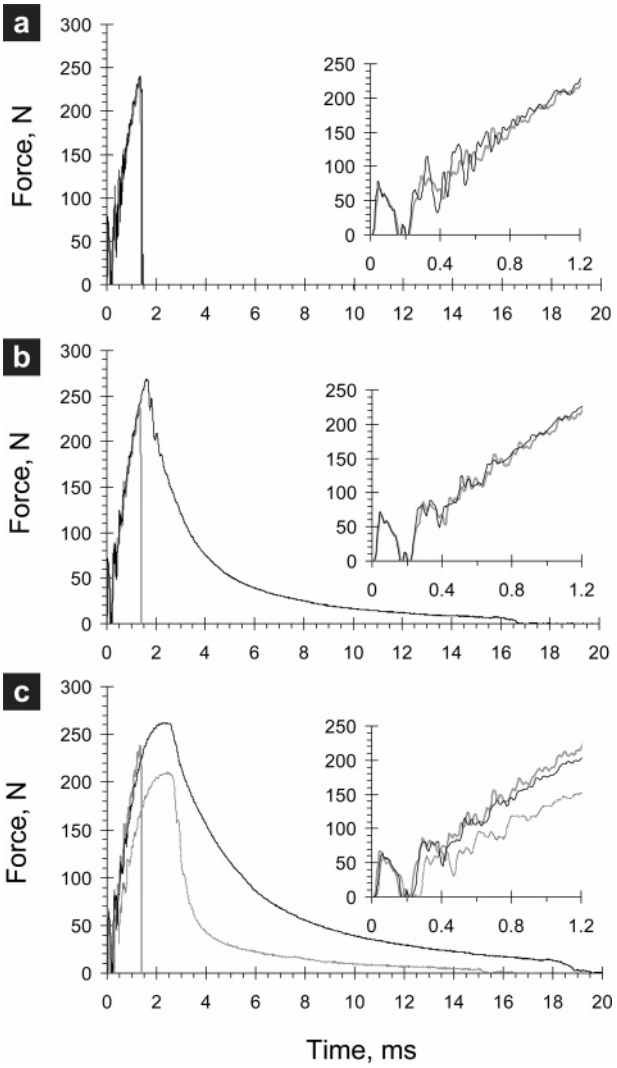

Figure 10. (a−c) Force vs time curves during impact testing for polyamide-12 toughened with 5, 10, and 20 wt % of SBM, respectively. Gray curves on each graph show the reference behavior of pure polyamide-12. Close-ups of the linear loading regime before crack initiation are given in the insets. The curve obtained with 20 wt % EPRm is reproduced in (c) with a black dotted line to highlight the differences observed between EPRm and SBM fillers.

Force measurements are given in Figure 10. The addition of 5 wt % SBM has no noticeable effect on the load, as inferred from visual observations. However, with 10 and 20 wt %, failure is clearly stable as also suggested by the pictures of crack surfaces. The maximum force at break as well as the dissipated impact energy increase significantly. With 20 wt % filler, the area under the load curve is much larger for SBM than for EPRm toughened specimens, as shown in Figure 10c. In terms of impact strength, a value of 60 kJ/m^2 is obtained with 20 wt % EPRm while it is of about 110 kJ/m^2 with 20 wt % SBM. Such difference in impact strength could be correlated to post-mortem observations. The whitened volume where most of the plastic deformation occurred is much larger with SBM than with EPRm. Higher magnification images of the fracture surfaces are given by SEM micrographs in Figure 11. They show that plastic deformation is much less pronounced with EPRm (Figure 11a) than with SBM (Figure 11b) fillers. In both systems, voids indicate that particle cavitation occurred during the impact. However, these voids are scarcely deformed in the case of EPRm, while cavities have largely expanded and matrix ligaments are elongated in the system filled with SBM.

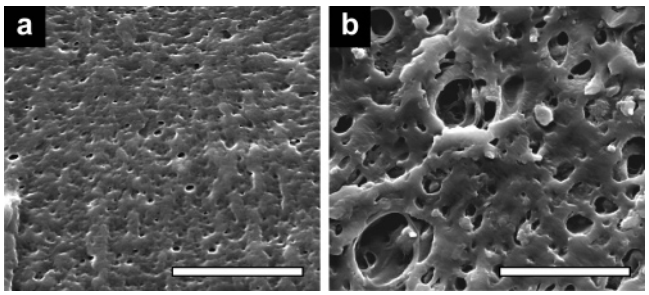

Figure 11. SEM observations of the crack surface of polyamide-12 (a) toughened with 20 wt % EPRm and (b) toughened with 20 wt % SBM (scale bar = 10 μm).

Unlike with EPRm, polyamide toughened with SBM exhibits little softening as illustrated in the inset of Figure 10c. Even with 20 wt % SBM, the impact stiffness is scarcely reduced compared to the important softening observed with 20 wt % EPRm. Parts a and b of Figure 12 show the impact stiffness and flexural modulus, respectively, as a function of filler concentration. For a given filler, both quantities decrease rather linearly with increasing filler content. However, the slope is much steeper with EPRm than with SBM. For a given filler content, the loss in impact strength (flexural modulus) caused by SBM is 80% (70%) smaller than the loss caused by EPRm. In the next section, we discuss how these values relate to the 36 wt % rubber content in SBM.

Impact Performances at Low Temperatures. Figure 13 shows the impact strength as a function of temperature for polyamide-12 systems unmodified and toughened with 20 wt % EPRm and SBM. Pure polyamide-12 is brittle in the whole temperature range with a rather constant impact strength of about 10 kJ/m^2. This value rises as the temperature reaches 30 °C, which is close to the glass transition temperature of polyamide-

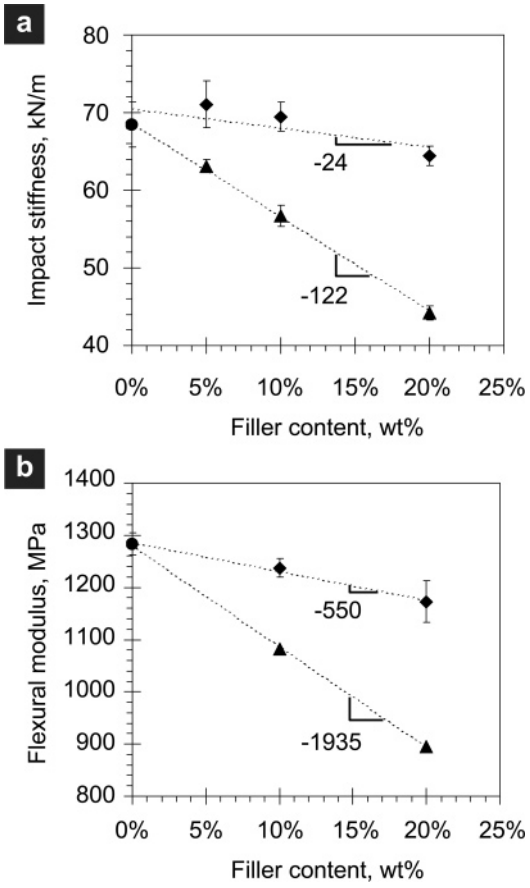

Figure 12. Impact stiffness of toughened polyamide-12 as a function of filler content: (a) impact stiffness; (b) flexural modulus (●, pure polyamide-12; ◆, with SBM fillers; ▲, with EPRm fillers). Numbers correspond to the slope of the dotted lines.

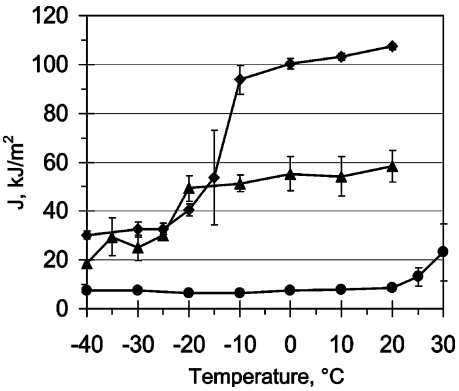

Figure 13. Notched Charpy impact strength, *J*, as a function of temperature (●, pure polyamide-12; ◆, with 20 wt % SBM fillers; ▲, with 20 wt % EPRm fillers).

12 (∼40 °C). Both toughened systems exhibit a much higher impact strength. At temperatures below −20 °C, samples globally have a brittle behavior. Impact strength is low (∼20−30 kJ/m^2), and the bursting failure suggests that crack propagation is unstable. At these temperatures, observations of post-mortem crack surfaces (not shown here) reveal that the very initiation of the crack is accompanied by cavitation and plastic deformation but rapidly switches to a brittle mode. A sharp brittle-to-ductile transition occurs at −20 °C for EPRm and −10 °C for SBM. Above these temperatures, failure is fully ductile. Samples do not break completely. Impact strength is much higher in SBM toughened materials than in pure polyamide-12. As observed at room temperature, samples filled with SBM (with impact strength of about 100 kJ/m^2) exhibit a much tougher behavior than with EPRm (impact strength of about 60 kJ/m^2).

Discussion

In the following, we focus on the blends containing 20 wt % of filler which all exhibit a ductile behavior. While both EPRm and SBM dispersions clearly show a toughening effect, they yield different impact performances. First, the impact strength is about twice larger with SBM than with EPRm fillers. In both cases, failure is ductile, crack propagation is stable, and impacted samples are not thrown far away from the testing device. These observations indicate that most of the energy lost by the hammer is converted into plastic work. Hence, the corresponding values of impact strength are directly related to the extent of plastic deformation. Post-mortem observations in Figure 5c and Figure 9c show that the whitened volume is about twice larger with the SBM than with the EPRm dispersion. Such difference presumably arises from the different cavitation properties of EPRm and SBM particles. In terms of toughening, cavitation is necessary to trigger the plastic deformation of the matrix. As a result, plastic deformation and thus energy dissipation are restricted to the volume where particles have cavitated. In particular, it has been shown that particle size is a key parameter for cavitation.[25] The stress required to induce cavitation in submicron-sized rubber particles increases as the particle size decreases. As a consequence, the extent of plastic deformation and thus the impact strength are reduced when the particle size decreases. Such phenomenon has already been observed in polyamide-6 toughened with various rubber fillers.[6,24,42] The authors show the existence of a minimum particle diameter—of the order of 0.2 μm at room temperature—below which the impact strength drops substantially. For instance, Oshinski et al. report that the Izod impact strength of polyamide-6 toughened with SEBS rubbers drops from 1000 to 400 J/m when particle diameter decreases from 0.4 to 0.1 μm. Here, EPRm particles ($d_n \approx 0.1$ μm) are about 4 times smaller than SBM ones ($d_n \approx 0.35$ μm), and the impact strength is about twice smaller. These similar trends suggest that the difference in impact strength between EPRm and SBM toughened polyamide is probably due to a size effect.

However, it should be noticed that not only the particle size but also the rubber nature and the filler nanostructure play a role on void formation.[13,16,18,24] Here, the SBM block copolymer is not reactive so that debonding may occur at the particle/matrix interface. However, TEM and SEM observations (not given here) at the boundary of the damaged whitened regions far from the crack surfaces suggest that voiding inside the SBM particles occurs prior to debonding at the interface. The choice of ABC block copolymer fillers may be of particular importance for the mechanisms of void formation. In nanostructured SBM particles, cavitation in the rubber domains may still occur, but the rubber B blocks may also provide a modulus contrast that facilitates debonding of brushes' interfaces. In particular, S brushes are little entangled considering the low molecular weight of the S blocks (≈30 000 g/mol) with respect to the molecular weight between entanglements of PS (≈20 000 g/mol). Therefore, S domains may act as weak interfaces that could easily open forming voids and locally relieving the hydrostatic stress. The present results do not allow us to validate such a mechanism, which shall be the subject of further investigation.

From a general point of view, many theoretical studies showed that a slight variation in the cavitation stress, whatever its origin is, has an important effect on the extent of plastic

deformation. As a rough estimate, one can consider the stress distribution in front of a crack of width w and length a submitted to a remote stress, σ^∞, normal to the crack surface (mode I). In the linear elastic approximation (LEFM), the hydrostatic stress, σ, decreases with the distance from the crack tip, r, and scales as follows:[41]

$$\sigma \sim \sigma^\infty \left(\frac{a}{r}\right)^{1/2} \tag{3}$$

Prefactors depending on the geometry of the crack are omitted. We introduce σ_c as the minimum stress required to induce cavitation in the fillers. It depends on several factors inherent to the materials (particle size, particle nanostructure, ...) and to the testing conditions (impact speed, temperature, ...). Knowing σ_c, no cavitation should occur at a distance greater than r_c which obeys

$$r_c \sim a\left(\frac{\sigma^\infty}{\sigma_c}\right)^2 \tag{4}$$

Thus, filler cavitation takes place in a volume V_c given by

$$V_c \sim w r_c^{\,2} \sim w a^2 \left(\frac{\sigma^\infty}{\sigma_c}\right)^4 \tag{5}$$

As a consequence, a 10% increase in the cavitation stress would induce a 40% reduction in the cavitated volume which, in turn, could have large repercussions on the extent of plastic deformation and on the dissipated energy.

Another important difference between EPRm and SBM fillers concerns the elastic modulus of toughened systems. As mentioned in the Introduction, it should be mostly determined by the rubber content and not by the filler content. Graphs in Figure 14 confirm these expectations. The impact stiffness and flexural modulus of all the studied systems are plotted as a function of rubber content in parts a and b of Figure 14, respectively. On both graphs, all data points align rather well on a same curve, suggesting that the rubber content is a controlling parameter. Considering only the rubber volume fraction, Φ_r, a good fit is obtained with the discrete particle model of Kerner as shown in Figure 14b. In this model, the overall Young modulus, E, is expressed by[10,12]

$$E = E_m \gamma \frac{(1-\Phi_r)E_m + \beta(\alpha+\Phi_r)E_r}{(1+\alpha\Phi_r)E_m + \alpha\beta(1-\Phi_r)E_r}$$

with $\alpha = (8 - 10\nu_m)/(7 - 5\nu_m)$, $\beta = (1 + \nu_m)/(1 + \nu_r)$, and $\gamma = (1 + \nu)/(1 + \nu_m)$, where ν_m, ν_r, and ν are the Poisson ratios of the matrix, the rubber, and the blend, respectively. We choose $\nu_r = 0.5$ for the rubber and $\nu = \nu_m = 0.4$ for the polyamide-12 matrix.[43] E_m is the Young's modulus of the matrix and E_r the Young's modulus of the rubber. Here, the flexural modulus is approximated to the Young's modulus. A least-squares method gives 1307 and 8 MPa for the fitting variables E_m and E_r, respectively, which is in good agreement with experimental values of 1400 and 1−2 MPa for the Young's moduli of polyamide-12 and polybutadiene rubber, respectively.[43] For SBM systems, this calculation assumes that the polystyrene (S) and poly(methyl methacrylate) (M) blocks have the same modulus as the polyamide matrix. However, at the high strain rates of impact testing, the elastic moduli of S and especially M are substantially higher than that of polyamide. This could explain why in Figure 14a the impact stiffness of SBM toughened systems is slightly higher than what would be obtained with rubber only.

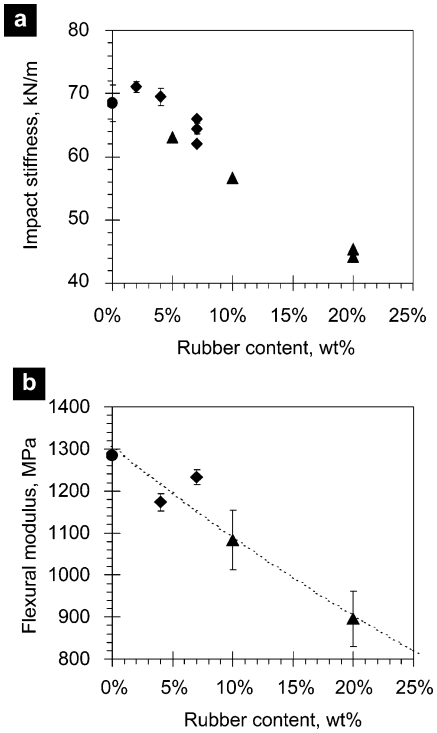

Figure 14. Effect of rubber content on the elastic modulus of toughened polyamide-12. (a) Impact stiffness as a function of rubber content. (b) Flexural modulus as a function of rubber content. The dotted line indicates the prediction given by the Kerner model ($\nu_r = 0.5$, $\nu = \nu_m = 0.4$, $E_m = 1307$ MPa, $E_r = 8$ MPa) (●, pure polyamide-12; ◆, with SBM fillers; ▲, with EPRm fillers).[31]

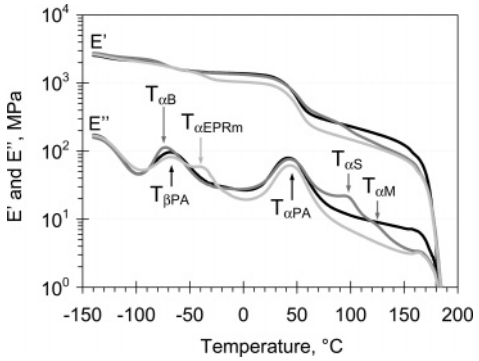

Figure 15. Dynamic mechanical analysis of toughened polyamide-12. Evolution of the storage, E', and loss, E'', moduli as a function of temperature at 1 Hz. Arrows indicate the α (glass) and β transitions of each component (black, pure polyamide-12; gray, with 20 wt % SBM; light gray, with 20 wt % EPRm).

This stiffening effect of the glassy S and M blocks is supported by dynamical mechanical analysis. Figure 15 shows the storage, E', and loss, E'', modulus as a function of temperature for three systems of polyamide-12: pure and filled with 20 wt % EPRm and 20 wt % SBM. The different states of the polyamide-12 matrix appear distinctly. The storage modulus drops step by step as the sample undergoes the β transition at about −70 °C, the glass (α) transition at 40 °C, and melting at 175 °C. In the presence of EPRm or SBM fillers, the signature of each component is clearly revealed by their glass transitions at −80 °C for B, −40 °C for EPRm, 90 °C for S, and 120 °C for M. In particular, it is possible to track how the S and M blocks contribute to the overall modulus of SBM toughened polyamide-12. Close-ups of Figure 15 are given with a linear

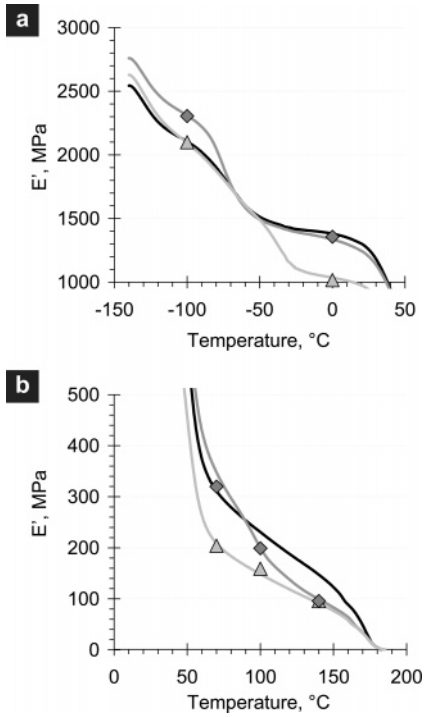

Figure 16. Close-ups of Figure 15. (a) Low-temperature range below glass transition of polyamide-12. (b) High-temperature range above glass transition of polyamide-12 (black, pure polyamide-12; gray, with 20 wt % SBM; light gray, with 20 wt % EPRm). Data points show the results of the Kerner model (◆, with 20 wt % SBM; ▲, with 20 wt % EPRm). Numerical data for the Kerner model at −100 °C: $E'_{EPRm} = E'_B = 2$ GPa, $E'_S = 3.5$ GPa, $E'_M = 5$ GPa; at 0 °C: $E'_{EPRm} = 150$ MPa, $E'_B = 1$ MPa, $E'_S = 3$ GPa, $E'_M = 3.5$ GPa; at 70 °C: $E'_{EPRm} = E'_B = 1$ MPa, $E'_S = E'_M = 2$ GPa; at 100 °C: $E'_{EPRm} = E'_B = E'_S = 1$ MPa, $E'_M = 1.5$ GPa; at 140 °C: $E'_{EPRm} = E'_B = E'_S = E'_M = 1$ MPa.

scale in Figure 16a,b to better show the different regimes. In the whole temperature range, the loss modulus is several orders of magnitude smaller than the storage modulus. Hence, the storage modulus can reasonably be approximated to the Young's modulus. The Kerner model given by (6) can be used to predict the overall storage modulus of multicomponent systems.[10,12] The storage moduli at different temperatures of S, B, M, and EPRm are taken from model experiments on homopolystyrene (M_n = 100 kg/mol, $I_p = 2.1$) and homopoly(methyl methacrylate) (M_n = 45 kg/mol, $I_p = 2.3$) and from various sources in the literature.[43−45] Poisson ratios are chosen equal to 0.35 for glassy components, 0.5 for rubbery ones, and 0.4 for the semicrystalline polyamide matrix. Calculated data points are reported in parts a and b of Figure 16 for EPRm and SBM toughened polyamide-12, respectively. They are in very good agreement with the experimental values, which suggests the following picture.

Below −80 °C, all the components are glassy. In this temperature range, polyamide-12, EPRm, and B have comparable moduli (∼2000 MPa), but S and especially M are much stiffer (∼3000 and 5000 MPa, respectively). As a result, the storage modulus is about the same for pure and EPRm toughened polyamide while it is 200 MPa higher for SBM toughened polyamide, as shown in Figure 16a. The situation changes above $T_{\alpha B}$ (−80 °C) and $T_{\alpha EPRm}$ (−50 °C) when EPRm and B become rubbery. Between −80 and 40 °C, SBM no longer acts as a stiffening agent. Still, because of the low B content of SBM, softening is much less pronounced than with pure EPRm rubber. These results reproduce qualitatively the three-point bending measurements given in Figure 14b. Above $T_{\alpha PA}$ (40 °C), the storage modulus of polyamide drops of about 1 decade while S and M are still glassy as shown in Figure 16b. The matrix becomes softer than the SBM particles so that the overall modulus of SBM toughened polyamide is slightly higher than that of pure polyamide. As temperature passes above $T_{\alpha S}$ (90 °C) and $T_{\alpha M}$ (120 °C), the storage modulus of SBM particles decreases progressively. Ultimately, at 140 °C, all three S, B, and M blocks are rubbery so that the matrix is filled with 20 wt % of pure rubber. Accordingly, both curves for SBM and EPRm toughened polyamide superimpose perfectly.

In summary, our study shows that block copolymer fillers can be used to separate advantageously the effects of rubber on toughness and elastic modulus. In addition, the present results in polyamide-12 are supported by comparable performances obtained in other polyamide-6 and polyamide-11 matrices with similar SBM fillers. The overall elastic modulus of toughened systems is mostly determined by the volume fraction of rubber while toughening requires that the matrix be sufficiently confined and that particles can cavitate to relieve the hydrostatic stress. Both critical matrix confinement and particle cavitation are dependent on the matrix and filler properties (particle size and structure, matrix crystalline organization, interfacial adhesion, ...) which are in turn strongly sensitive to processing conditions. Hence, generally, block copolymers with low rubber content should constitute efficient impact fillers provided that their dispersion and nanostructure fit the toughening criteria in terms of matrix confinement and cavitation. In this context ABC triblock copolymers and in particular SBM block copolymers seem to be a material of choice.

Conclusion

SBM copolymers containing less than 40 wt % of rubber can have great toughening effects without altering significantly the elastic modulus when being dispersed in polyamide-12. Even though SBM and polyamide-12 are not compatibilized, droplet coalescence was shown to be substantially hindered during blending. The polyamide systems toughened with these SBM dispersions exhibit an impact strength and elastic modulus that are both much higher than those obtained in the same polymer matrix filled with pure rubber particles (EPRm). We consider the separate effects of rubber on the toughening mechanisms on one side and on the elastic modulus on the other to explain these results. By introducing glassy blocks, it is possible to reduce the overall rubber content and thereby to attenuate the loss in elastic modulus while toughening remains efficient as long as void formation occurs. In nanostructured particles of ABC block copolymers such as SBM, void formation may be driven by various molecular mechanisms. Whether it arises from cavitation inside the rubber B domain or from debonding of weakly entangled brushes in the glassy S domains is an open question that is worth further studies. The present results also suggest that the overall elastic modulus could even be enhanced by using glassy blocks that are stiffer than the matrix. The promising performances of SBM toughened polyamide-12 do not pretend to be optimal in any way. We believe that they rise several interesting issues and perspectives. What minimum rubber content is required, how the filler nanostructure affects the blend properties, and how the nature of the glassy blocks affects the overall elastic modulus are some of these questions.

Acknowledgment. We thank Patrick Coupard and Cyrille Mathieu (Arkema) for their help and advice about microscopy. We are also grateful to Stéphane Jouenne, Anne-Valérie Ruzette (ESPCI, CNRS), and Nicolas Amouroux (Arkema) for helpful discussions about instrumented impact testing and DMA.

Authors are indebted to Prof. H. E. H. Meijer for stimulating discussions and comments. Financial support from CNRS, ESPCI, and Arkema is gratefully acknowledged.

References and Notes

(1) Epstein, B. N. U.S. Patent 4,174,358, 1979.
(2) Kinloch, A. J.; Young, R. J. *Fracture Behaviour of Polymers*, 2nd ed.; Elsevier Applied Science: London, 1985.
(3) Keskkula, H.; Paul, D. R. Toughened nylons. In *Nylon Plastics Handbook*; Kohan, M. I., Ed.; Hanser: Munich, 1995; pp 414−434.
(4) Akkapeddi, M. K. Rubber toughening of polyamides by reactive blending. In *Reactive Polymer Blending*; Baker, W., Scott, C. E., Hu, G.-H., Eds.; Hanser: Munich, 2001; pp 207−252.
(5) Modic, M. J.; Pottick, L. A. Modification and compatibilization of nylon 6 with functionalized styrenic block copolymers. *Polym. Eng. Sci.* **1993**, *33*, 819−826.
(6) Oshinski, A. J.; Keskkula, H.; Paul, D. R. The role of matrix molecular weight in rubber toughened nylon 6 blends. *Polymer* **1996**, *37*, 4919−4928.
(7) Kayano, Y.; Keskkula, H.; Paul, D. R. Fracture behaviour of some rubber-toughened nylon 6 blends. *Polymer* **1998**, *39*, 2835−2845.
(8) Tanrattanakul, V.; Hiltner, A.; Baer, E.; Perkins, W. G.; Massey, F. L.; Moet, A. Toughening PET by blending with a functionalized SEBS block copolymer. *Polymer* **1997**, *38*, 2191−2200.
(9) Bassani, A.; Pessan, L. A. Toughening of polypropylene with styrene/ethylene-butylene/styrene triblock copolymer. *J. Appl. Polym. Sci.* **1997**, *86*, 3466−3479.
(10) Kerner, E. H. The elastic and thermo-elastic properties of composite media. *Proc. Phys. Soc. B* **1956**, *69*, 808−813.
(11) Uemura, S.; Takayanagi, M. Application of the theory of elasticity and viscosity of two-phase systems to polymer blends *J. Appl. Polym. Sci.* **1966**, *10*, 113−125.
(12) Bandyopadhyay, G. G.; Bhagawan, S. S.; Ninan, K. N.; Thomas, S. Viscoelastic behaviour of polypropylene/nitrile rubber thermoplastic elastomer blends: Application of Kerner's models for reactively compatibilized and dynamically vulcanized systems *J. Polym. Sci., Part B* **2004**, *42*, 1417−1432.
(13) Borggreve, R. J. M.; Gaymans, R. J.; Schuijer, J.; Ingen Housz, J. F. Brittle-tough transition in nylon-rubber blends: effects of rubber concentration and particle size. *Polymer* **2004**, *28*, 1489−1496 .
(14) Wu, S. Phase structure and adhesion in polymer blends: A criterion for rubber toughening. *Polymer* **1985**, *26*, 1855−1863.
(15) Borggreve, R. J. M.; Gaymans, R. J.; Eichenwald, H. M. Impact behavior of nylon rubber blends: 6. Influence of structure on voiding processes—toughening mechanism. *Polymer* **1989**, *30*, 78−83.
(16) Hobbs, S. Y.; Dekkers, M. E. Deformation mechanisms in toughened poly(phenylene oxide)-polyamide blends. *J. Mater. Sci.* **1989**, *24*, 1316−1322.
(17) Muratoglu, O. K.; Argon, A. S.; Cohen, R. E.; Weinberg, M. Microstructural fracture processes accompanying growing cracks in tough rubber-modified polyamides. *Polymer* **1995**, *36*, 4787−4795.
(18) Kim, G. M.; Michler, G. H. Micromechanical deformation processes in toughened and particle filled semicrystalline polymers. Part 1: Characterization of deformation processes in dependence on phase morphology. *Polymer* **1998**, *39*, 5689−5697.
(19) Kim, G. M.; Michler, G. H. Micromechanical deformation processes in toughened and particle filled semicrystalline polymers. Part 2: Model representation for micromechanical deformation processes. *Polymer* **1998**, *39*, 5699−5703.
(20) van der Wal, A.; Gaymans, R. J. Polypropylene-rubber blends: 5. Deformation mechanism during fracture. *Polymer* **1999**, *40*, 6067−6075.
(21) Argon, A. S.; Cohen, R. E. Toughenability of polymers. *Polymer* **2003**, *44*, 6013−6032.
(22) Fukui, T.; Kikuchi, Y.; Inoue, T. Elastic-plastic analysis of the toughening mechanism in rubber-modified nylon: matrix yielding and cavitation. *Polymer* **1991**, *32*, 2367−2371.
(23) Dijkstra, K.; Bolscher, G. H. T. Nylon-6 rubber blends: 3. Stresses in and around rubber particles and cavities in a nylon matrix *J. Mater. Sc.* **1994**, *29*, 4286−4293.
(24) Dijkstra, K.; van der Wal, A.; Gaymans, R. J. Nylon-6 rubber blends: 4. Cavitation and yield in nylon rubber blends. *J. Mater. Sc.* **1994**, *29*, 3489−3496.
(25) Lazzeri, A.; Bucknall, C. B. Applications of a dilatational yielding model to rubber-toughened polymers. *Polymer* **1995**, *36*, 2895−2902.
(26) Tzika, P. A.; Boyce, M. C.; Parks, D. M. Micromechanics of deformation in particle-toughened polyamides. *J. Mech. Phys. Solids* **2000**, *48*, 1893−1929.
(27) Bartczak, Z.; Argon, A. S.; Cohen, R. E.; Weinberg, M. Toughness mechanism in semicrystalline polymer blends: II. High-density polyethylene toughened with calcium carbonate filler particles. *Polymer* **1999**, *40*, 2347−2365.
(28) Schrauwen, B. A. G.; Govaert, L. E.; Peters, G. W. M.; Meijer, H. E. H. The influence of flow-induced crystallization on the impact toughness of high-density polyethylene. *Macromol. Symp.* **2002**, *185*, 89−102.
(29) Corté, L.; Beaume, F.; Leibler, L. Crystalline organization and toughening: example of polyamide-12. *Polymer* **2005**, *46*, 2748−2757.
(30) Corté, L.; Leibler, L. On dispersions of block copolymer droplets. *Macromolecules* **2006**, *39*, 2445−2448.
(31) Rebizant, V. Reactive SBMX block copolymers: synthesis, structuration and toughening of vitreous matrices Ph.D. Thesis Université Pierre et Marie Curie, Paris, 2003.
(32) Rebizant, V.; Venet, A.-S.; Tournilhac, F.; Girard-Reydet, E.; Navarro, C.; Pascault, J.-P.; Leibler, L. Chemistry and mechanical properties of epoxy-based thermosets reinforced by reactive and nonreactive SBMX block copolymers. *Macromolecules* **2004**, *37*, 8017−8027.
(33) Corté, L.; Leibler, L. Analysis of polymer blend morphologies from transmission electron micrographs. *Polymer* **2005**, *46*, 6360−6368.
(34) Ireland, D. R. Instrumented impact testing. *ASTM-STP* **1974**, 463.
(35) Radon, J. C. Application of instrumented impact test in polymer testing. *J. Polym. Sci.* **1978**, *22*, 1569−1581.
(36) Instrumented impact testing of plastics and composite materials. *ASTM STP* **1987**, 936.
(37) Slavin, S. E.; Beswick, G. T. Instrumented Izod impact testing. *J. Polym. Sci.* **1993**, *49*, 1065−1070.
(38) Savadori, A. Impact testing of plastics—present knowledge. *Polym. Test.* **1985**, *5*, 209−241.
(39) Vu-Khanh, T. Determination of the impact fracture parameters in ductile polymers. *Polymer* **1988**, *29*, 1979−1984.
(40) Mai, Y.-W.; Powell, P. Essential work of fracture and J-integral measurements for ductile polymers. *J. Polym. Sci., Part B: Polym. Phys.* **1991**, *29*, 785−793.
(41) Broberg, K. B. *Cracks and Fracture*; Academic Press: Cambridge, 1999.
(42) Oostenbrink, A. J.; Molenaar, L. J.; Gaymans, R. J. *6th Annual Meeting of Polymer Processing Society*; Nice, 1990.
(43) *Polymer Handbook*, 4th ed.; Brandrup, J., Immergut, E. H., Grulke, E. A., Eds.; Wiley: New York, 1999.
(44) Carlberg, M.; Colombini, D.; Maurer, F. H. J. Morphology and viscoelastic properties of EPR/PDMS blends. *J. Appl. Polym. Sci.* **2004**, *94*, 2240−2249.
(45) Mohsin, M. A.; Berry, J. P.; Treloar, L. R. G. Dynamic-mechanical properties of polybutadiene rubbers. *Polymer* **1985**, *26*, 1463−1468.

MA061090G